DOI: 10.1002/ ((please add manuscript number))
Article type: Full Paper

Neuromorphic organic devices that specifically discriminate dopamine from its metabolites by non-specific interactions

*Martina Giordani, Matteo Sensi, Marcello Berto, Michele Di Lauro, Carlo Augusto Bortolotti, Henrique Leonel Gomes, Michele Zoli, Francesco Zerbetto, Luciano Fadiga, Fabio Biscarini**

Martina Giordani, Prof. Michele Zoli
Dipartimento di Scienze Biomediche, Metaboliche e Neuroscienze, Centro di Neuroscienze e Neurotecnologie (CFNN) - Università di Modena e Reggio Emilia, Via Campi 287, 41125 Modena (Italy)

Dr. Matteo Sensi, Dr. Marcello Berto, Dr. Carlo Augusto Bortolotti, Prof. Fabio Biscarini
Dipartimento di Scienze della Vita - Università di Modena e Reggio Emilia, Via Campi 103, 41125 Modena (Italy)
E-mail: fabio.biscarini@unimore.it

Dr. Michele Di Lauro, Prof. Luciano Fadiga, Prof. Fabio Biscarini
Center for Translational Neurophysiology - Istituto Italiano di Tecnologia, Via Fossato di Mortara 17-19, 44100 Ferrara (Italy)

Prof. Henrique Leonel Gomes
Instituto de Telecomunicações, Avenida Rovisco, Pais 1, 1049-001 Lisboa (Portugal)

Prof. Henrique Leonel Gomes
Universidade do Algarve, Faculdade de Ciências e Tecnologia, 8005-139 Faro (Portugal)

Prof. Francesco Zerbetto
Dipartimento di Chimica "G. Ciamician", Università di Bologna, Via F. Selmi 2, 40126 Bologna (Italy)

Prof. Luciano Fadiga
Dipartimento di Scienze Biomediche e Chirurgiche Specialistiche, Sezione di Fisiologia, Università di Ferrara, Via Fossato di Mortara 17-19 44100 Ferrara (Italy)

Keywords: biosensors, organic bioelectronics, PEDOT:PSS, short-term plasticity, neuromorphic devices

Abstract: Specific detection of dopamine (DA) is achieved with organic neuromorphic devices with no specific recognition function towards DA in an electrolyte solution. The response to voltage pulses consists of amplitude-depressed current spiking that mimics the short-term plasticity (STP) of neuronal synapses. A simple equivalent circuit hints that the STP timescale

of the device arises from capacitance and resistance of the PEDOT:PSS layer in series with the electrolyte resistance. Both capacitance and resistance of PEDOT:PSS change with the composition of the buffer solution. Dose curves are constructed from the STP characteristic timescale for each DA metabolite across a range of molar concentrations from 1 pM to 1 mM. Remarkably, STP response of DA is distinctive with respect to the other metabolites even when the latter differ from DA only by one functional group. Both the STP timescale and the sensitivity to DA solutions are two-to-five times larger across the patho-physiological range (0.1-10 nM) with respect to those of the solutions with DA metabolites. Density Functional Theory calculations on clusters hint to a stronger hydrogen bond pattern of DA ammonium end group compared to that of the cationic metabolites. The exponential correlation between the experimental STP timescale and the binding energy of DA metabolites interacting with PEDOT:PSS indicates that the slow dynamics of ionic species in and out PEDOT:PSS upon voltage pulsing is the origin of the neuromorphic STP response of the device. Our sensing framework can discriminate differences of non-specific interactions with the active material as small as a few kcal/mol, else corresponding to one functional group in the molecular structure.

1. Introduction

Dopamine (DA) is a neurotransmitter of the catecholamine family synthesized in dopaminergic neurons that control diverse functions, such as locomotion, reward and neuroendocrine secretions. The degeneration of dopaminergic neurons causes a decrease of DA concentration in caudate-putamen extracellular fluid (ECF) (whose composition is similar to the one of the cerebrospinal fluid (CSF)). DA level decrease below 50% in caudate-putamen is a main pathogenic feature of Parkinson's disease (PD),[1] characterized by motor and non-motor symptoms.[2] Current therapeutic strategies for PD focus on reducing the severity of motor symptoms via systemic administration of DA precursor L-DOPA[3], or by deep-brain

stimulation[4]. In the perspective of personalized medicine or loco-regional treatment of PD it is therefore important to quantitatively detect DA in vivo and real time.

DA detection poses several challenges: i) the ultra-low DA concentration in ECF/CSF, that decreases down to 200 pM in PD;[5] ii) DA lability as it is rapidly oxidized to neuromelanin when exposed to light and oxygen;[6] iii) the presence of interfering agents, and iv) other catecholamines and catabolites derived from the metabolism of DA, that share most of its chemical features and are present at comparable concentration. The metabolic reactions in the brain tissue are depicted in **Figure 1** and the physiological levels in healthy humans are reported in **Table 1**.

Much of the work on DA detection relies on electrochemical techniques. The discrimination of DA with respect to other substances exhibiting similar redox potentials, like ascorbic acid (AA) or uric acid (UA) present at (tens) micromolar concentration in ECF and CSF, can be difficult.[7,8] Nafion-coated carbon electrodes are used for electrochemical detection of DA, as the polyanion Nafion screens out ascorbate and urate from faradic reactions.[9]

An alternative to electrochemistry is sensing with organic electronics devices. Organic Electrochemical Transistors (OECTs) based on poly(3,4-ethylenedioxythiophene):poly-styrenesulfonate (PEDOT:PSS), were used to perform fast scan cyclic voltammetry,[10] to monitor the change of transconductance due to DA oxidation[11] or to the variations of electrical characteristics in the presence of different concentrations of DA.[7] Another work demonstrated label-free DA detection with Electrolyte-Gated Organic Field-Effect Transistors (EGOFETs), with DA bound irreversibly to a phenylboronic acid, immobilized on the gate electrode, by means of a condensation reaction.[12] In all these reports, the discrimination from other metabolites was not assessed.

Organic devices operated in a two- or three-terminal architecture with voltage pulses at fixed amplitude and frequency produce an output current response with either increasing or

decreasing amplitude depending on the frequency.[13] These devices can also mimic the response of neuronal synapses, embodying in one device some of the functions of neural circuitry, such as short term plasticity (STP), spike-timing-dependent plasticity (STDP), long term potentiation (LTP) and long term depression (LTD).[14,15] These features are attractive for developing artificial intelligence on the one hand, and prosthetic integration into the brain circuitry on the other hand.

Recently, we proposed to exploit the STP response of organic neuromorphic devices as a new label-free sensing framework for molecular solutes. The idea behind it is that the STP timescale depends on the interaction between PEDOT:PSS and the molecular solutes present in solution.[16,17] We demonstrated detection of DA with limit of detection (LOD) ca 1 pM in the co-presence of either AA or UA. The key factor for discrimination was ascribed to the fact that PEDOT:PSS exchanges cations (DA dominant form at physiological pH is cationic) whereas it is much less prone to intake anions (both AA and UA are present as their conjugated bases). This simple, yet effective, approach that discriminates promptly the net charge of molecules interacting with PEDOT:PSS allowed us to circumvent the limitation of cyclovoltammetry for DA detection in the presence of UA and AA.[18]

In this paper, we demonstrate the specific label-free detection of DA with respect to the products of its catabolism and other catecholamine neurotransmitters produced by DA metabolic routes. This set of molecules is a challenging breadboard as they share comparable masses and charges, are present at ultra-low concentration levels in ECF and CSF and differ from one another only by a single functional group. In particular, at physiological pH, DA, 3-methoxytyramine (3-MT), norepinephrine (NE) and epinephrine (EPI) bear the same positive charge in the ammonium group,[19] and differ because of mono-methylation of the catechol (3-MT), the presence of hydroxyl group in beta position of the chain (NE and EPI), and methylation of the amino group (EPI).

The main result is that the STP response of our organic neuromorphic device to DA exhibits always longer STP timescales than the response to its catabolites and other catecholamine neurotransmitters. This implies that the device is sensitive not only to the presence of ionic charges, but also to more subtle differences in non-covalent interactions, each of a few kcal/mol. DFT calculations on a small cluster model of PEDOT:PSS rationalize the observed trend of STP timescales, offering a simple explanation in terms of changes in hydrogen bonding and pi-stacking motives. Conversely, we find that the neuromorphic device is insensitive to 3,4-dihydroxyphenylacetic acid (DOPAC) and homovanillic acid (HVA) that according to their pK_a are anionic catabolites at physiological pH. This is expected by analogy with the sensing response of our device towards AA and UA.[16,17]

The paper is organized as follows: in Sect. 2 we describe the experimental methods and the details of the data analysis and computational models; in Sect. 3 Results and Discussion we first present the experimental results obtained with the neuromorphic device (Sect. 3.1); we describe the results of the DFT calculations on cluster models of PEDOT:PSS and the DA/metabolite (Sect. 3.2); then we show and explain the correlation between the experimental timescales (related to the DA/metabolite concentration) and the binding energy between PEDOT:PSS and the DA/metabolite by invoking the kinetic Eyring theory; in section 3.4 we reproduce the experimental STP response using a simple equivalent circuit, where we identify two components, i.e. the interfacial resistance and capacitance of PEDOT:PSS, are both sensitive to the concentration of DA/metabolite; finally in Sect 4 we draw the conclusions.

Table 1. Physiological concentrations of DA and DA metabolites in extracellular fluid (ECF) and cerebrospinal fluid (CSF).

Molecule	**Concentration (M)**		**Refs.**
	ECF	**CSF**	
Dopamine (DA)	$1.0\text{x}10^{-9} – 3.0\text{x}10^{-8}$	$9.0\text{x}10^{-11}$	[5],[20]
3-Methoxytyramine (3-MT)	$4.0\text{x}10^{-9}$	$2.0\text{x}10^{-8}$	[3],[21],[9]
Homovanillic Acid (HVA)	$1.0\text{x}10^{-6}$	$1.5\text{x}10^{-7}$	[4,22],[9]
3,4-Dihydroxyphenylacetic Acid (DOPAC)	$1.0\text{x}10^{-6}$	$2.8\text{x}10^{-7}$	[4],[9]
Norepinephrine (NE)	$2.8\text{x}10^{-10}$	$3.7\text{x}10^{-10}$	[23],[24]

Epinephrine (EPI)	$1.8x10^{-10}$	$1.5x10^{-10}$	[25],[24]

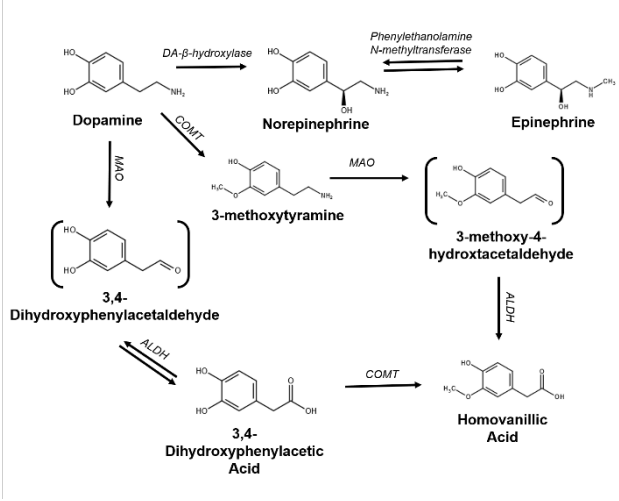

Figure 1. Dopamine catabolism is produced by a set of enzymes (monoamine oxidase – MAO-, cathecol-O-methyl transferase -COMT- and aldehyde dehydrogenase - ALDH -) that act in sequence producing dihydroxyphenylacetic acid, 3-methoxytyramine and homovanillic acid. DA is also precursor of norepinephrine and epinephrine by enzymatic reactions catalyzed by dopamine β-hydroxylase and phenylethanolamine N-methyltransferase.

2. Experimental

2.1. Fabrication and characterization of the device

The neuromorphic device (**Figure 2**) consists of two PEDOT:PSS electrodes (large area electrode, 0.12 mm^2 and a small area electrode, 0.04 mm^2) bridged by phosphate buffer solution (PBS) 50mM pH 7.4 as electrolyte containing either DA, or a catabolite, or a neurotransmitter (see **Figure S1**, Supporting Information). All reagents were purchased from Sigma-Aldrich, except PEDOT:PSS from Ossila Ltd (Sheffield, UK). Films of PEDOT:PSS are spin cast on a flexible and transparent substrate made of polydymethylsiloxane (PDMS) (Figure 2a-step1) then surface treated with N_2 plasma for 5 min (Figure 2a step 2).[16,17] The PDMS substrate (thickness 80 μm) is obtained through spin coating of 0.1 ml/cm^2 of Sylgard 184 (Dow Chemicals, Delaware) at 500 rpm for 3 minutes (Figure 2a-step 3). The electrodes are drawn with computer aided design (CAD) software (Figure S1a, Supporting Information) and then patterned on PEDOT:PSS film by laser ablation with a short-pulsed Nd:YAG laser (center

wavelength 1064 nm, pulse width 10 ns, peak power 3 kW) using the laser scan marker *ScribaR* (Scriba Nanotecnologie S.r.l., Bologna, Italy) (Figure 2a-step 4).[26,27]

The device operations are inspired by STP in neural circuitry.[28] With reference to Figure 2b, the larger electrode acts as pre-synaptic terminal and it is pulsed with a train of unipolar voltage pulses for 1 s (0.5 s of initial delay and 0.5 s of measurements) at a frequency of 500 Hz with -200 mV voltage amplitude; the small electrode is used to record the resulting displacement current, thus acting as a post-synaptic terminal. The electrical measurements are performed with an Agilent B2912A Source Measure Unit in ambient condition and in a Faraday cage with triaxial connectors yielding a 4 pA base noise level. In Figure 2c is shows the fabricated sensor, that is flexible and can be stretched and bent.

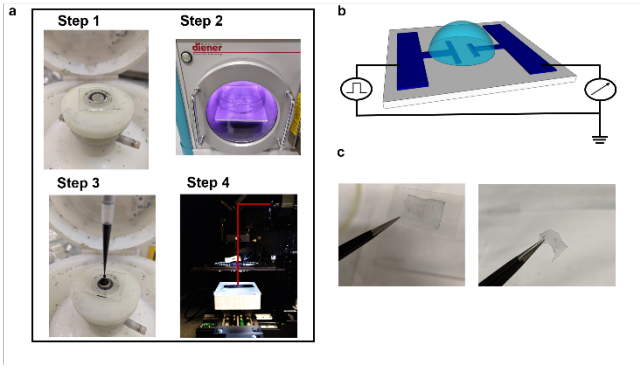

Figure 2. a) Fabrication processes: step 1 – spin coating of PDMS; step 2 – N_2 plasma; step 3 – spin coating of PEDOT:PSS; step 4 – laser ablation. b) Schematic drawing of the neuromorphic device with details on stimulation/current measurement; c) the sensor is flexible and can be stretched and bent.

2.2. Computational details

Density Functional Theory (DFT) calculations were performed using the PBE[29] functional as implemented in the TURBOMOLE suite of programs.[30] The resolution-of-identity (RI) technique has been used to speed up computations. Def-SVP basis set has been adopted for all atoms. To obtain reliable results in terms of geometry, orbital distribution and energy values, we performed geometry optimizations in implicit solvent (water) with Screening Model

(COSMO) approach:[31] the system was solvated in water by setting the dielectric constant equal to 80. We adopted the empirical D3 dispersion correction proposed by Grimme[32] to describe dispersion forces that are relevant to the model. Molecular orbitals and energy values for PEDOT (charge +1) and PSS (charge -1) models are in good agreement with previous works for describing the polaron state.[33,34] The Mulliken charges distribution of the system showed that most of the negative charge (-0.64) in PSS is localized on the sulfonate anion. Then, starting from PEDOT and PSS models, we converged to an optimized PEDOT:PSS model.

2.3 Analysis of the sensor response

The maxima of the displacement current exhibit a depressive behavior that is fitted with the exponential envelope function:

$$I_{env}(t) = I_{\infty} + \Delta I_0 \cdot e^{-t/\tau_{STP}} \quad (1)$$

I_{∞} is the long-time plateau, $I_{\infty}+\Delta I_0$ is the current response to the first voltage pulse, t is the time from that of the first voltage pulse t_0, and τ_{STP} is the characteristic relaxation time of the depressive response.[17] From best fit of the peaks by the function equation 1 we obtain τ_{STP}, that is the parameter correlated with the concentration of DA in the solution. To build dose curves, we measured STP response and hence extracted τ_{STP} at different concentrations from 1 pM to 1 mM for DA, with concentration intervals of one order of magnitude between data points. We repeated the procedure for each molecule listed in Table 1 at all its concentrations. To reduce the device-to-device difference and compare the data, we normalized the signal S to the $\tau_{STP,0}$ of the STP response of the device in presence of the sole PBS, as shown in **Equation 2**:[35]

$$S = \frac{(\tau_{STP} - \tau_{STP,0})}{\tau_{STP,0}} \quad (2)$$

We used the same fitting as in **Equation 1** for interpolating all the minima and the average, which is estimated as the mean value between maxima and minima current at each pulse. We found that the value of τ_{STP} is nearly the same.

3. Results and discussion

3.1 Comparison of STP response of DA and its metabolites

Figure 3 shows the experimental pulses and STP current response of a representative organic neuromorphic device. Monophasic (negative) rectangular voltage pulses v_A(t) (blue line in Figure 3a) are generated at the pre-synaptic electrode. The external applied voltage waveform generates a corresponding current waveform i_S (t) measured at the post-synaptic electrode. Initially, the current pulses have their origin at zero amps, however, with the application of subsequent pulses the current waveform begins to drift towards more negative values (Figure 3a red line). Figure 3b shows the behavior of the current upon the application of a very long train of voltages pulses. The envelope of the current peaks, both maxima and minima, decays rapidly within a few pulses and approaches a saturation limit after the application of several pulses. This behavior is often reported in the literature of neuromorphic devices.[28,36,37]

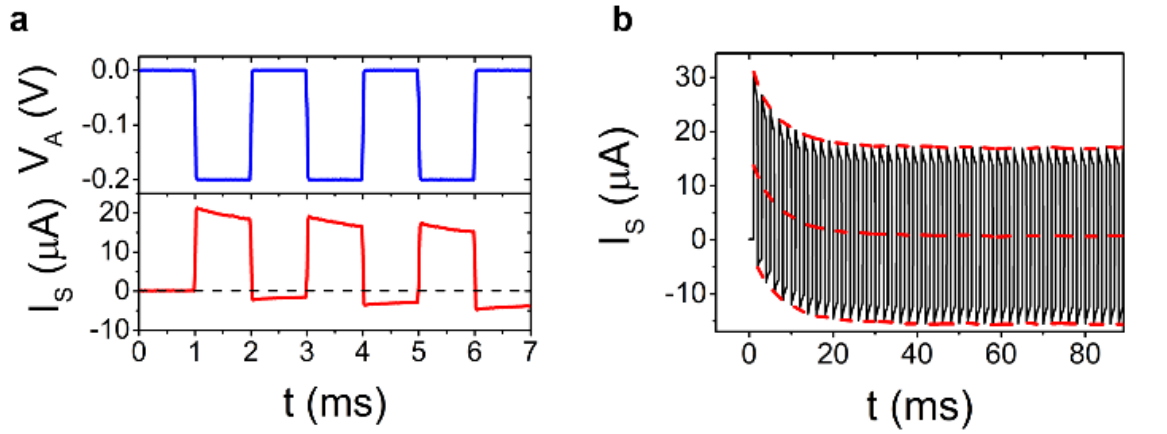

Figure 3. STP response of the neuromorphic device: (a) top blue line, the square voltage pulses generated by the pre-synaptic electrode; bottom red line, the current pulses produced at the post-synaptic electrode after application of voltage pulses. Notice the drift of the current base line and the current spikes, both drifting towards more negative values; (b) transient in the current waveform upon the application of unipolar voltage pulses at 500 Hz. Dashed red lines are the

envelopes of the maxima, minima, and average value of the current peaks. In this case the best fit values according to eq.1 are: τ_{STP} = 7.40 ± 0.01 ms, I_∞ = 1.6777 $\cdot 10^{-5}$ ± 8$\cdot 10^{-10}$ A and ΔI_0 = 1.568 $\cdot 10^{-5}$ ± 2$\cdot 10^{-8}$ A for the upper envelope, τ_{STP} = 7.66 ± 0.01 ms, , I_∞ = 0.574 $\cdot 10^{-6}$ ± 5$\cdot 10^{-10}$ and ΔI_0 = 1.412 $\cdot 10^{-5}$ ± 1$\cdot 10^{-8}$ A for the average envelope and τ_{STP}=7.54 ± 0.01 ms, I_∞ = -1.5628 $\cdot 10^{-5}$ ± 7$\cdot 10^{-10}$ A and ΔI_0 = 1.347 $\cdot 10^{-5}$ ± 1$\cdot 10^{-8}$ A for the lower envelope.

We observed that the STP response timescale is modulated when a solute, that has a strong interaction with PEDOT:PSS, is introduced. Initially, the solute is partitioned between the solution and the electrodes. The first voltage pulse moves one of the electrodes out of equilibrium, causing either outflow or inflow (depending on the voltage sign) of ionic species at the polymeric electrode. Depending on the strength of the interaction, we expect the STP timescale to become greater as the interaction with the solute and its concentration gets larger.

In **Figure 4** we show the signal *S* vs concentration for DA and its metabolites, that are depicted in Figure 1. For sake of clarity, in Figure 4a we overlay the dose curves of DA with the ones from cationic species,[19] namely NE, 3-MT and EPI. Instead, Figure 4b provides the comparison between the same DA dose curve as in Figure 4a and the dose curves of anionic catabolites, DOPAC and HVA. We notice that the signal *S* associated to the presence of DA is always larger than the signal obtained in the presence of any metabolite, regardless of the net charge of the prevailing form, and also that the cations produce larger signal values than anions. Focusing on Figure 4a, the fact that the dose curve of DA is always well above that from the cationic metabolites indicates a longer retention time across the whole range. It should also be noticed that both NE and 3-MT exhibit dose curves with a trend similar to that of DA, although they are shifted down vertically. Moreover, NE is always above the values of 3-MT. As the two catecholamines have similar pK_a values, we can infer that the methylation in 3-MT has a role in decreasing the interaction with PEDOT:PSS, with respect to NE. A possible reason is the steric hindrance of methyl group that weakens pi-stacking and prevents additional H-bond formation with the hydroxyl of the catechol group. The dose curve for EPI exhibits smoother

variation, thus suggesting that the sterically hindered ammonium group in the secondary catecholamine is weakly coupled to PEDOT:PSS.

The comparison between DA and the anionic catabolites DOPAC and HVA in Figure 4b supports our expectations, i.e., that the anionic catabolites exhibit much shorter retention times and their curves are largely superimposed, thus indicating that the interaction of both DOPAC and HVA with the electrode is rather non-specific.

To quantify the trends of the dose curves, we fit the signal *S vs* the molar concentration *C* of each substance as:

$$S = 1 - \exp\left[-\left(\frac{C}{C_0}\right)^n\right] \tag{3a}$$

whose first non-zero term is the power-law for $\frac{C}{C_0} \ll 1$:

$$S \approx \left(\frac{C}{C_0}\right)^n \tag{3b}$$

Hence the timescale can be approximated as:

$$\tau_{STP} \approx \tau_0\left[1 + \left(\frac{C}{C_0}\right)^n\right] \tag{3c}$$

The characteristic molar concentration C_0 and the exponent *n* are two fitting parameters whose best fit values extracted from the linear fit of *lnS* vs *lnC* in **Equation 3**b, together with the estimated errors, are reported in **Table 2**. One can immediately notice that these parameters are characteristic of each metabolite and that the larger values of $1/C_0$ correlates with the longer characteristic timescales, in particular DA>NE>3-MT>DOPAC>HVA>EPI. According to equation 3a, C_0 represents an upper limit of detection, since the signal tends to saturation for $C \gg C_0$.

The sensitivity of each dose curve is estimated as the derivative of the best fit curve in Figure 4, viz. $\frac{dS}{dC} \approx \frac{n}{C_0}\left(\frac{C}{C_0}\right)^{n-1}$ hence is concentration-dependent. Because of the exponent n<1, the largest sensitivity is achieved at the lowest concentrations. Thus, in Table 2 we report the sensitivity values at the two limits of the patho-physiological concentration range of DA, viz.

100 pM and 10 nM. At the lower concentration, the sensitivity for DA, 3-MT, NE, is similar, while for EPI is one order of magnitude smaller.

Comparing the response to DA to the ones to HVA and to DOPAC in the patho-physiological concentration range, we observe that the dose curve response shows about 4 times lower sensitivity to the anionic form at physiological pH with respect to DA. This behavior is consistent with the one observed in our previous work with AA and UA.[17]

The DA curve also reveals a theoretical limit of detection, calculated as the mean blank signal value + three times the associated standard deviation, lower than 1 pM (while the lowest DA concentration tested is 1 pM) and 2-4 times larger sensitivity in the whole patho-physiological concentration range (from 100 pM to 10 nM) with respect to cationic catabolites or other catecholamine neurotransmitters.

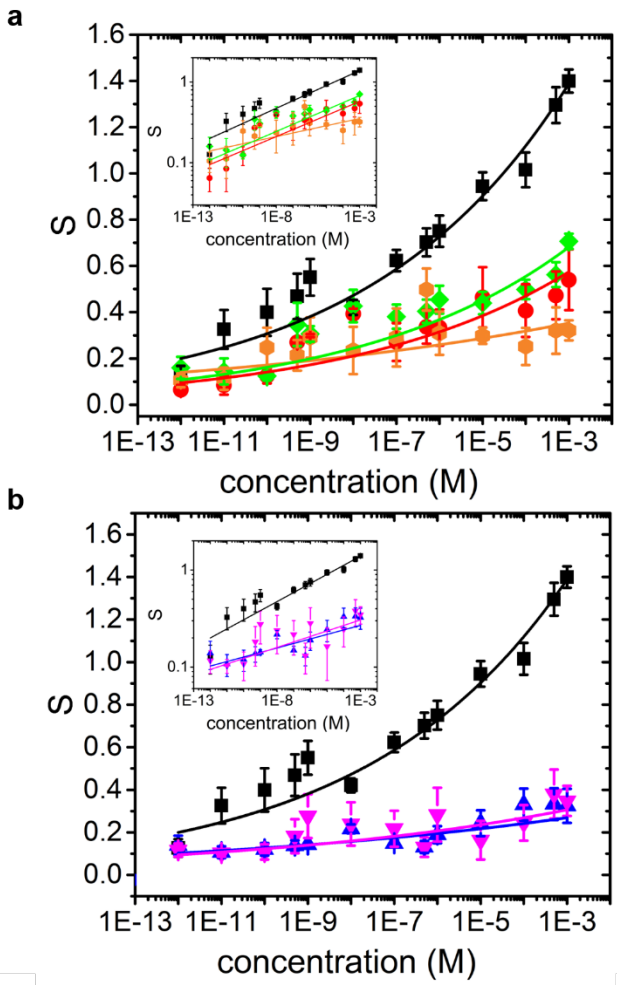

Figure 4. Signal *S*, lin-log plots for concentrations of DA (black squares) vs (a) cationic: 3-MT (red circles), NE (green lozenges) and EPI (orange hexagons), and (b) anionic catabolites: DOPAC (pink inverted triangles) and HVA (blue triangles). Error bars correspond to the SEM of S averaged over five devices. Continuous lines are functions $S=(C/C_0)^n$, where the parameters C_0 and n are obtained from linear regression as $\ln S=(-n\cdot\ln C_0)+n\cdot\ln C$. The insets in Figure 4 showing the log-log plots of the main overlays evidence that the exponent n of DA, 3-MT, and NE takes similar values, the one of EPI is smaller, as well as the ones of the anionic catabolites DOPAC and HVA.
In summary the ordering of n is DA≈ 3-MT ≈ NE >DOPAC≈HVA>EPI.

Table 2. Sensitivity in the patho-physiological range to the different DA catabolites, and best fit parameters of the dose curves.

Molecule	*Sensitivity at 100 pM (M^{-1})*	*Sensitivity at 10 nM (M^{-1})*	*$\ln(C_0/M)$ $\pm\,\delta\ln(C_0/M)$*	*n*
DA	2.9E+08	4.4E+06	-4.56±0.34	0.089±0.05
3-MT	1.4E+08	2.2E+06	-0.55±1.66	0.087±0.01
NE	1.6E+08	2.2E+06	-0.89±0.69	0.079±0.01
EPI	7.7E+07	9.4E+05	10.21±2.40	0.034±0.01
HVA	5.9E+07	7.3E+05	7.21±1.85	0.051±0.01
DOPAC	7.0E+07	9.0E+05	4.93±1.18	0.059±0.01

3.2 Correlation between binding energies and STP timescales

A molecular scale explanation of the observed selectivity of the STP response can be given by relating the timescales to non-equilibrium phenomena of transport and interaction within PEDOT:PSS. PEDOT:PSS exhibits an extended active interface with the electrolyte, that involves the whole volume. This characteristics was studied by Rivnay and co-workers and termed “volumetric capacitance of PEDOT:PSS”.[38] At the outer interface with the electrolyte, PSS^- acts as a surfactant and does not contribute to the hole conductivity. Ion diffusion there occurs on a fast time-scale, the non-equilibrium state generated by the voltage pulses being then rapidly re-equilibrated. Conversely, at the PEDOT:PSS/electrolyte interface which lies deeper inside the film, where hole conduction takes place, ion diffusion is slowed down because of the longer pathways from the free electrolyte solution and constricted environment. The consequence is that a longer time is needed for the system to attain again equilibrium once it has been displaced from it upon a voltage pulse. If the time between pulses is short, the system cannot relax back to the absolute minimum of free energy, thus, pulse after pulse, the current drifts and the capacitance slowly changes. The out of equilibrium population at PEDOT:PSS interface produces the drift of conductance in time of the device. These arguments hint to the capacitance as the main contributor to the timescale τ_{STP} of the envelope Equation 1. This explanation seems consistent with the discussion reported later in Section 3.3.

The interaction of PEDOT:PSS with catabolites affects the timescale for their desorption from the active layer, hence the time scale that is exponentially related to the desorption free energy ΔG_{des} is exponentially contributed by the binding energy E_b of the molecule to PEDOT:PSS, in other words the enthalpic term $\Delta H_{des}=-E_b$ of the reaction PEDOT:PSS/DA -> DA + PEDOT:PSS.

Following the kinetic Eyring theory, in the transition state type of approach, a generic rate constant, ν, can be written as

$$\nu \propto exp\left(-\frac{\Delta G_{des}}{RT}\right) = exp\left(+\frac{\Delta S_{des}}{R}\right) \cdot exp\left(-\frac{\Delta H_{des}}{RT}\right) = exp\left(+\frac{\Delta S_{des}}{R}\right) \cdot exp\left(+\frac{E_b}{RT}\right) \qquad (4)$$

where the enthalpic term can be obtained by quantum chemical calculations of the purely electronic energies E_b. We then establish how E_b changes with the nature of the DA derivative. For this, we performed a DFT calculation, adopting a cluster model of the polymer with three styrene sulfonate (SS) and three monomers of 3,4-ethylenedioxythiophene (EDOT). The central SS is in the anionic form, offering a SO_3^- group towards PEDOT, while two lateral SS are protonated (SO_3H). Both PEDOT and PSS are truncated and capped with methyl groups. In this system, the overall charge is taken as 0, since PEDOT has a formal charge +1 and PSS -1. Defining the geometry of PEDOT:PSS is not trivial, therefore we first optimized the geometry of the single monomers and then used the resulting structures as starting point for optimizing the geometry of the pair.

The results of the DFT calculation show that for this minimum PEDOT:PSS model, the HOMO-LUMO energy gap is small (<1 eV), underlining the conductive character of the polymer. The HOMO and LUMO orbitals are mainly localized on PEDOT (see **Figure S2**). The binding energy of PSS^- to $PEDOT^+$ in water, calculated as the total energy of PEDOT:PSS minus the sum of the total energies of $PEDOT^+$ and of PSS^-, is -26.5 kcal/mol.

To elucidate the mechanism, we investigated the binding of DA and other catabolites to PEDOT:PSS. In particular, we focused the attention of DFT calculations on the catabolites that are cations at the operational experimental pH (7.4). DA, NE and 3-MT feature a positively charged ammonium group. For this reason, we evaluated the electrostatic interaction and hydrogen bonds (H-bonds) formation between the sulfonate anion of PSS and the ammonium group of the catabolites.

In the initial geometry of the PEDOT:PSS/DA system, we placed the N atom of ammonium in DA 4.5 Å away from the sulfonate anion of PSS. Upon optimization in implicit solvent, the three H atoms of the ammonium group form three H-bonds: one with an oxygen of the central sulfonate anion, one with an oxygen of a lateral sulfonate and the last one with an oxygen atom of PEDOT (see **Figure 5** and **Table 3** for distances). As shown in Figure S2, the binding of the DA cation induces a decrease of the negative charge on PSS and an increase of positive charge on PEDOT, whose charge is less effectively compensated by PSS. The HOMO of the solvated system decreases upon DA binding and is partially localized on DA.

With same starting configuration, we then investigated the binding geometries and energies of 3-MT, NE, and EPI to PEDOT:PSS (Figure 5 and Table 3). Three H-bonds with PEDOT:PSS are also formed by 3-MT and NE. However, these H-bonds exhibit longer distances than those with DA, suggesting the presence of weaker bonds. EPI, which presents a methylated amine, can form only one weak bond with PSS. If we compare charges and orbitals of PEDOT:PSS with and without the catabolites (see figure S2), we can conclude that in our model, the PEDOT:PSS system is affected more by DA binding than by binding to the other catabolites and neurotransmitters.

As shown in Table 3, DA has the highest binding energy (-23.3 kcal/mol) to PEDOT:PSS, few kcal/mol more than 3-MT (-21.6 kcal/mol) and NE (-19.9 kcal/mol). EPI has much smaller binding energy, -9.3 kcal/mol, in line with the trend observed with charges and orbitals energies. These differences can be understood in terms of the contributions of the three H-bonds of the ammonium ion: in the case of 3-MT, the H-bond to the central SS- elongates substantially, while in the case of NE are the two side H-bonds to SSH and PEDOT that are weakened by the elongation. In the case of EPI, only the H-bond with SS^- forms. Calculations show that EPI has a much weaker interaction with PEDOT:PSS in agreement with the experimental data. The strong non-covalent binding, due to the interactions between the ammonium group of catecholamines and the sulfonate group is a conserved feature for the ammonium-terminated

metabolites. The similar binding energies and charge distributions in the models where PEDOT:PSS is bound to DA, 3-MT or NE, suggest that the longer DA retention observed experimentally may be ascribed to other contributions, like π-stacking and cation-π interactions. The results of DFT calculations evidence that DA forms the strongest bond with PEDOT:PSS. The ordering of the (absolute value of the) binding energy to PEDOT:PSS is

DA> 3-MT>NE>EPI.

This sequence resembles the ordering of $1/C_0$ - and n- values fitting the dose curves from STP response.

3.3 Origin of the STP timescale.

We attempt a simple explanation for the origin of the observed STP timescales. Following kinetic Eyring theory, we can envision that the timescales governing the dynamics of ions interacting with a solid matrix arise from a distribution of free energy barriers, where the binding energy E_b is assumed to be the dominant enthalpic contribution. By neglecting possible differences in the entropic contribution and assuming that desorption of DA or metabolite is the rate limiting step, one expects at any concentration that an Arrhenius dependence between C_0 and E_b holds. We first write the STP time scale (in terms of frequency ν) as emerging from the thermal average of individual processes governed by the Arrhenius dependence:

$$\langle \nu \rangle = \frac{1}{\tau_{STP}} = \frac{h}{RT} \sum_{sites\ i=1}^{N} \frac{N_{occ,i}}{N} exp\left(-\frac{\Delta G_{des,i}}{RT}\right) \approx A \frac{h}{RT} \sum_{sites\ i=1}^{N} \frac{N_{occ,i}}{N} exp\left(+\frac{E_{b,i}}{RT}\right) \qquad (5)$$

where $\frac{N_{occ,i}}{N}$ is the fraction of PEDOT:PSS sites occupied with binding energy $E_{b,i}$; it also termed population or occupancy. A is a constant containing the entropic contributions. The occupancy is then dependent on the concentration C and on the presence of competitors/antagonists that can subtract the binding sites upon a much stronger binding (e.g. divalent cations). By fixing the composition of the electrolyte solution, and assuming that the occupancy is smoothly energy-dependent, we can approximate the occupancy as being just a

function of the concentration $\frac{N_{occ}}{N}(C)$ and neglect the variability with the specific site (energy).

For a large number *N* of sites, a continuous average can replace the sum in **Equation 5**:

$$\langle \nu \rangle = \frac{N_{occ}}{N}(C)\frac{h}{RT}\langle exp\left(-\frac{\Delta G_{des}}{RT}\right)\rangle \approx A\frac{N_{occ}}{N}(C)\frac{h}{RT}\langle exp\left(\frac{E_b}{RT}\right)\rangle =$$

$$A\frac{N_{occ}}{N}(C)\frac{h}{RT}exp\left\{\langle exp\left(\frac{E_b}{RT}\right)-1\rangle_c\right\} \qquad (6)$$

The *c* subscript of the right-most identity implies the averaging of the Arrhenius factor in terms of the cumulant average of the term in bracket.[39,40] The first terms of the cumulant expansion are:

$$\langle \nu \rangle = A\frac{N_{occ}}{N}(C)\frac{h}{RT}exp\left\{\frac{\langle E_b\rangle}{RT}\left[1-\frac{1}{2RT}\frac{\sigma^2}{\langle E_b\rangle}+\frac{1}{6(RT)^2}\left(\frac{\langle {E_b}^3\rangle-3\sigma^2\langle E_b\rangle-\langle E_b\rangle^3}{\langle E_b\rangle}\right)-\cdots.\right]\right\} \qquad (7)$$

The first term of the expansion in square brackets represents the "pure" Arrhenius behavior dependent only on the mean binding energy $\langle E_b \rangle$; the second term contains the second cumulant or variance $k_2=\sigma^2$ (square of the standard deviation σ); the third term is the third cumulant whose leading term is the skewness $\frac{\langle {E_b}^3\rangle}{\sigma^3}$. **Equation 6** states that the distribution of the binding energies (here described through its cumulants or combination of moments) introduces deviations from the "pure" Arrhenius behavior. The cumulants of order ≥2 quantify the "energy disorder". Based on this analogy, one we can state that "energy disorder" in the binding sites of the PEDOT:PSS layer introduces deviations from the expected 1/RT exponential rate. The consequence is that the exponential Arrhenius behavior transforms into a stretched exponential:

$$S \propto \tau_{STP} \propto exp\left[-\frac{1-f\left(\frac{\sigma^2}{\langle E_b\rangle},\ldots\right)}{RT}\langle E_b\rangle\right] \qquad (8)$$

For a symmetric (central) distribution of the binding energy (for instance, gaussian energy disorder), then the only cumulant beyond the mean $\langle E_b \rangle$ surviving is the variance σ^2; if the active material is highly ordered, viz. $\sigma \to 0$, the Arrhenius behavior is recovered because the function $f \to 0$. Noticeably, for a gaussian or central distribution of the binding energy there is not deviation from the Arrhenius behavior, as the binding energy disappears in the second

cumulant contribution and the cumulant correction enters only in the pre-exponential term. Then, it is non-central energy disorder with the third cumulant that introduces a non-Arrhenius correlation with the binding energy.

As we have described the signal *S* with the power law in equation 3b, then we expect a linear correlation of $-nlnC_0$ vs E_b, with the slope being smaller than the inverse thermal energy, that is 1.7 kcal/mol at RT, due to the energy disorder:

$$-nlnC_0 \propto -\frac{1-f\left(\frac{\sigma^2}{\langle E_b\rangle};\ldots\right)}{RT}\langle E_b\rangle \quad (9)$$

To confirm this prediction, in **Figure 6** we plot $-nlnC_0$ vs the binding energy $-E_b$ from DFT (which is not necessarily the closest estimate for $<E_b>$ because of the simplicity of our model). We observe a positive correlation whose estimated slope (from the dashed straight line) is about 0.06 mol/kcal, i.e. smaller than 1/RT as it should be for a "pure" Arrhenius model. The model we propose is therefore that PEDOT:PSS is a material with a distribution of sites with different binding energies for the tested metabolites (thus not only with one binding energy) which originates an exponential correlation between the "mean" binding energy and the measured timescale. The deviation from a pure Arrhenius model is due to the disorder of the binding energy distribution. Above all, this correlation hints that both the microscopic origin of the differential response, as well as the sensitivity and resolution of the device, depend on the subtle differences of the binding energies of each molecule of this study with PEDOT:PSS. Interestingly, our simple DFT model provides a reasonable insight on the origin of the specific response, in particular, it hints to possibility of distinguishing differences in the binding energy with PEDOT:PSS of just a few kcal/mol.

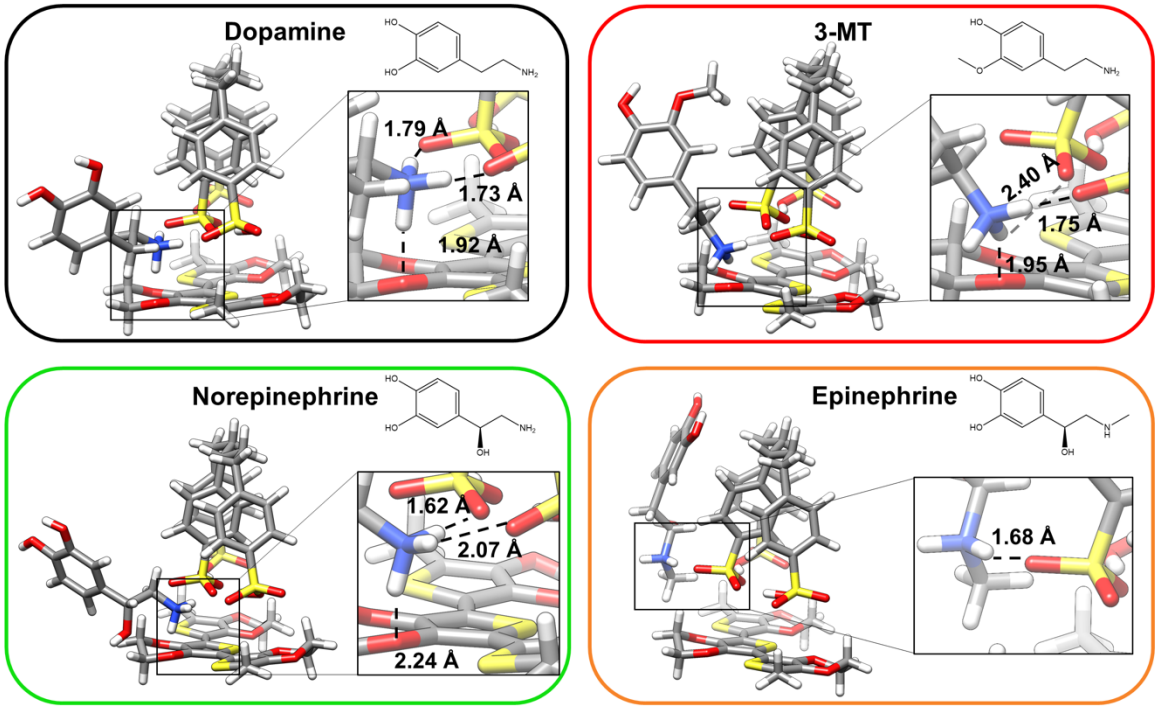

Figure 5. Binding of DA catabolites to PEDOT:PSS. Optimized structures of PEDOT:PSS and catabolites: DA, 3MT, NE and EPI.

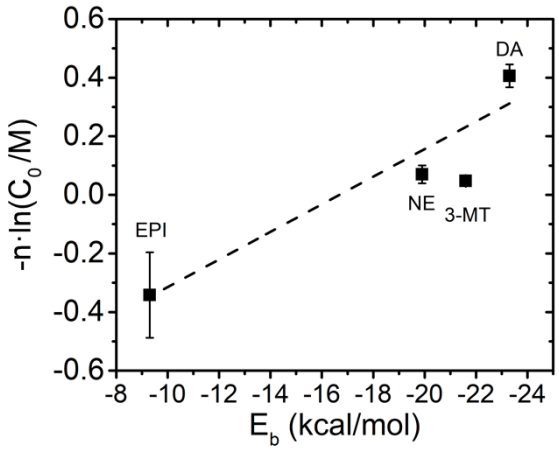

Figure 6. Correlation plot between the fitting parameters and the binding energy with PEDOT:PSS. The error bars are calculated from error propagation.

Table 3. Binding energies and bond distances for the interaction of the PEDOT:PSS model with DA and its cationic metabolites.

Catabolite bound to PEDOT:PSS	*Binding Energy (kcal/mol)*	*H-bonds*
DA	-23.3	-NH_3^+---O(SS^-) = 1.73 Å - NH_3^+---O(SSH) = 1.79 Å - NH_3^+---O(PEDOT) = 1.92 Å

3-MT	-21.6	- NH_3^+---O(SS-) = 2.40 Å* - NH_3^+---O(SSH) = 1.95 Å* - NH_3^+---O(PEDOT) = 1.75 Å
NE	-19.9	- NH_3^+---O(SS-) = 1.62 Å - NH_3^+---O(SSH) = 2.07 Å - NH_3^+---O(PEDOT) = 2.24 Å
EPI	-9.3	- NH_3^+---O(SS-) = 1.68 Å

3.4 STP response

Finally, we comment on the meaning of the STP response in Figure 3 using a simple equivalent circuit (**Figure 7**a), which allows us to establish a connection between macroscopic circuit properties and the microscopic interactions discussed in Section 3.2. The transient effect on the current waveform recorded at the post-synaptic terminal occurs because the input voltage signal is a short pulse. Here, short means that the period T of the input signal has to be shorter than 5 times the device time constant ($T<5\tau$). In circuit analysis, 5 τ is generally assumed as the time that must elapse after the impulse for the voltage across the capacitor to effectively reach the steady state. Upon these conditions the circuit requires several voltage pulses to reach the steady state, viz. the amount of charge flowing into the capacitor during charging half cycle equals the amount of charge flowing out of the capacitor during discharging half cycle.

By looking at the response to a few initial pulses at 500 Hz (Figure 3a), one notices that the relaxation to the initial baseline current is prevented by the onset of the next voltage pulse that produces a progressively lower mean current. Accordingly, the peaks of the displacement current occur with the same pulse frequency but exhibit a progressively smaller (positive) value and a larger (negative) value. For many pulses (Figure 3b), the envelopes of the peaks (maximum and minimum) exhibit an exponential decay in time to reach a plateau, and the mean current plateau is lower than the initial baseline current.

Since the transient effect shown in Figure 3b is used as the relevant property for sensing, it is important to understand how the STP transient of the current waveform is affected by the analyte concentration as well as by the physical device parameters, like pulse amplitude V_0,

duration Δt, frequency ν=1/T (T is the period), and number of pulses N_p. The duty cycle of the input signal is Δt /T.

To gain insight into the transient response observed, we chose to adopt an equivalent RC circuit, sketched in Figure 7a. The parallel network comprising the resistance R_D and capacitance C_D accounts for the region dominated by the large capacitance of the PEDOT:PSS/electrolyte interface, in series with the electrolyte region described here as the resistor R_E. In general, R_D and C_D are time-varying as a result of the dynamics of ions in and out of PEDOT:PSS. Hence, they are the most sensitive elements to the composition of the electrolyte solution as well as to the interactions of the solutes, the latter being dynamically partitioned between the solution and PEDOT:PSS. In order to obtain an analytical solution that reproduces the essential features of the sensing signals we take them as constant. We keep in mind, however, that even these "mean field" values must be regarded as characteristic of the nature of solute and concentration. A complete discussion on the choice of the components in the circuit, together with the exact solution as well as a dynamic model of ion-PEDOT:PSS interactions, will be presented elsewhere. Here we show that the circuit correctly predicts the transient response for a train of N_p square pulses.

When a single square voltage pulse is applied to the device, the overall current i_S (t) that flows through the system consists of two components, one resistive flowing through R_D and the other capacitive through C_D:

$$i_S(t) = \frac{v_C(t)}{R_D} + C_D \frac{dv_C(t)}{dt} \qquad (10)$$

To calculate i_s (t) one needs to solve the differential **Equation 10** for the voltage v_C (t). The analytical solution is given in terms of the time constant τ:

$$\tau = \frac{R_D R_E C_D}{R_D + R_E} \qquad (11)$$

Equation 11 is the time constant of an RC circuit with an effective resistance consisting of two in-series resistors.

The first pulse yields the voltage:

$$v_C(t) = V_0 \frac{R_D}{R_D + R_E}\left[1 - e^{-\frac{t}{\tau}}\right] \quad \text{for } 0 \le t \le \Delta t \qquad (12a)$$

$$v_C(t) = V_0 \frac{R_D}{R_D + R_E} e^{-\frac{t}{\tau}}\left[e^{\frac{\Delta t}{\tau}} - 1\right] \text{ for } \Delta t < t \le T \qquad (12b)$$

Equation 12a applies when the voltage pulse is on, viz. during charging, while equation 12b applies during the lag time when the capacitor is discharging. At the end of the first pulse, viz. at the period $T = 1/\nu$ where ν is the pulse repetition frequency, the residual voltage is:

$$v_C(T) = V_0 \cdot \frac{R_D}{R_D + R_E} \cdot e^{-\frac{T}{\tau}}\left(e^{\frac{\Delta t}{\tau}} - 1\right) \qquad (13)$$

This is the voltage at which the second pulse starts. We notice that only when $T \gg \Delta t$, the next pulse starts from $v_C(0)=0$ volt, else its value depends on the voltage divider (i.e. the two resistors), as well as on the ratio between τ and the frequency/duty cycle. The sign of $v_C(t)$ will be the same of the input pulse V_0.

For $N_p \ge 2$, a recursion solution is found. The voltage built upon $n+1=N_p$ pulses reads:

$$v_C(nT) = v_C(T)\left[\frac{1 - e^{-\frac{nT}{\tau}}}{1 - e^{-\frac{T}{\tau}}}\right] \qquad (14)$$

Equation 14 encompasses both **Equation 13** for n=1, and $v_C(0)$=0 V for n=0. Then the voltage $v_C(t)$ can be written as:

$$v_C(t) = v_C(nT) \cdot e^{-\frac{t-nT}{\tau}} + V_0 \frac{R_D}{R_D+R_E}\left[1 - e^{-\left(\frac{t-nT}{\tau}\right)}\right] \text{ for } nT \le t \le nT + \Delta t \quad (15a)$$

$$v_C(t) = \left[v_C(nT) + v_C(T)e^{\frac{T}{\tau}}\right] e^{-\frac{t-nT}{\tau}} \text{ for } nT + \Delta t < t \le (n+1)T \quad (15b)$$

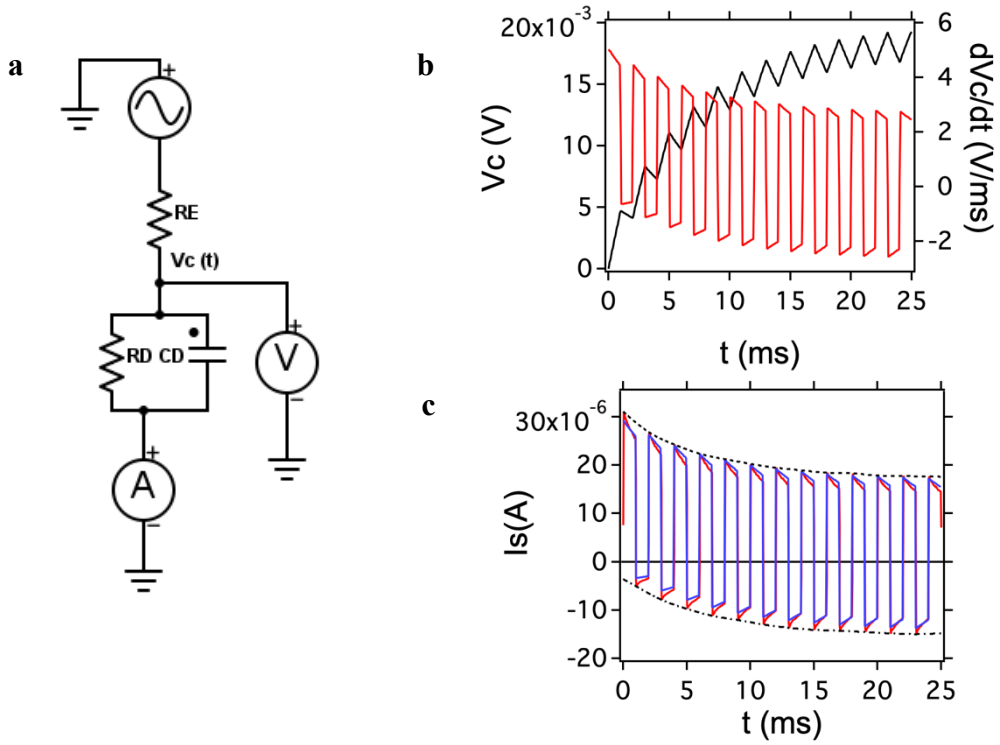

Figure 7. (a) The equivalent circuit adopted to describe the neuromorphic device exhibiting STP; the voltmeter measures the voltage $v_c(t)$; (b) time dependence of the voltage $v_c(t)$ across the capacitor from equation 13 (black line); the right axis shows the derivative obtained from equation 15 (red line); (c) STP current response from the equivalent circuit in (a) using equation 16 (blue line). Circuit parameters used are C_D=5.8μF, R_D=1.4 kΩ and R_E=15.0 kΩ. The experimental curve (red line) shows deviations in the details of each peak. Dashed black and dashed-dotted black lines are the envelopes of the experimental STP maxima and minima of each spike, respectively.

The combination of **Equations 15**a and 15b results in the voltage waveform plotted in Figure 7b left axis for an V = 37mV applied at the second electrode. The variance of this value with 0.2 V applied experimentally at the first electrode is ascribed to the oversimplification of the equivalent circuit in Figure 7a. The value found must be regarded as an effective potential that is divided across the network of the resistors in the circuit, also the ones not accounted for here,

as for instance contact and bulk resistances. We notice that the voltage rises and decays within a pulse has the same dynamics and the same time constant τ. The difference between the maximum and minimum voltages achieved at the pulse n+1 is then obtained by plugging $t=nT+\Delta t$ in equation 15a and $t=(n+1)T$ in Equation 15b (else taking Equation 14) respectively:

$$v_{C,max}(n) - v_{C,min}(n) = \left[v_C(nT) + v_C(T)e^{\frac{T}{\tau}}\right] \cdot \left[e^{-\frac{\Delta t}{\tau}} - e^{-\frac{T}{\tau}}\right] \tag{16}$$

Equation 16 shows that this difference, that determines the current spike amplitude, can be maximized with the input frequency and duty cycle. It is also evident that the envelope passing through the maxima (obtained from Equation 15a) or the minima (as from Equation 15b) exhibits an exponential trend, whose characteristic time scale equals τ.

To obtain the current, we need first to calculate the derivative of Equation 15 shown in Figure 7b, right axis:

$$\frac{dv_C(t)}{dt} = \left[\frac{V_0}{\tau}\frac{R_D}{R_D+R_E} - \frac{v_C(nT)}{\tau}\right] e^{-\left(\frac{t-nT}{\tau}\right)} \text{for } nT \le t \le nT + \Delta t \tag{17a}$$

$$\frac{dv_C(t)}{dt} = -\frac{v_C(t)}{\tau} \qquad \text{for } nT + \Delta t < t \le (n+1)T \tag{17b}$$

then we combine Equations 15a (b) and 17a (b) into Equation 10 to yield:

$$i_S(t) = \frac{V_0}{R_D+R_E} - \left[\frac{V_0}{R_D+R_E} - \frac{V_0}{R_E} + \frac{v_C(nT)}{R_E}\right] e^{-\frac{t-nT}{\tau}} \text{ for } nT \le t \le nT + \Delta t \tag{18a}$$

$$i_S(t) = -\frac{v_C(t)}{R_E} = -\frac{\left[v_C(nT)+v_C(T)e^{\frac{T}{\tau}}\right]}{R_E} e^{-\frac{t-nT}{\tau}} \quad for\ nT + \Delta t < t \le (n+1)T \tag{18b}$$

In Figure 7c we show the current waveform as obtained from **Equation 18** for the following parameters: C_D=5.8 μF, R_E=1.4 kΩ, and R_D=15.0 kΩ. The time constant equation 11 is τ=7.4 ms in agreement with the value obtained by best fit. We compare it first to the time derivative $dv_c(t)/dt$ of the potential (right axis in Figure 7b) to infer that the trend is largely dictated by the capacitive contribution to the current equation 10, however the shape of the current spike and the exponential trend within each peak is more affected by the resistive contributions and fails to closely follow the details. Noticeably, by comparing it to the envelope fitted on the recorded current in Figure 3b (reported in Figure 7c as a dashed line), we find an excellent agreement. Maxima and minima of each current spike read:

$$i_S(nT+\Delta t) = i_{S,min} = \frac{V_0}{R_D+R_E} - \left[\frac{V_0}{R_D+R_E} - \frac{V_0}{R_E} + \frac{v_C(nT)}{R_E}\right] e^{-\frac{\Delta t}{\tau}} \quad (19a)$$

$$i_S\big((n+1)T\big) = i_{S,max} = -\frac{\left[v_C(nT)e^{-\frac{T}{\tau}} + v_C(T)\right]}{R_E} \quad (19b)$$

Noticeably, the inverse exponential decay rate of either the maxima or the minima from **Equation 19**, are both equal to the inverse time decay rate of $v_C(nT)$ in Equation 13, viz. τ. Thus, we infer that our observable from the current peaks envelope is $\tau_{STP} \approx \tau$. This justifies our choice to relate τ_{STP} to the solute composition, as we stated that, even in this simplistic equivalent circuit description of the device, C_D and R_D are to be regarded as composition-sensitive circuit elements.

A few final considerations are useful:

i) by choosing T=2 ms, compared to τ=7.4 ms, it is necessary to supply $N_p \geq 5\,\tau/T \approx$ 18 pulses to achieve the steady state, in agreement with Figure 3b;

ii) the maximum STP is quantified as the difference between the maximum peak current at $t=\Delta t$ and the maximum at the steady state for $t=nT$ with n>>18:

$$\Delta i_S = i_S(\Delta t) - \lim_{n\to\infty} i_S(nT + \Delta t) = \frac{V_0}{R_D+R_E} - \left[\frac{V_0}{R_D+R_E} - \frac{V_0}{R_E}\right] e^{-\frac{\Delta t}{\tau}} -$$

$$-\frac{V_0}{R_D+R_E} + \lim_{n\to\infty}\left[\frac{V_0}{R_D+R_E} - \frac{V_0}{R_E} + \frac{v_C(nT)}{R_E}\right] e^{-\frac{\Delta t}{\tau}} = \lim_{n\to\infty}\frac{v_C(nT)}{R_E} e^{-\frac{\Delta t}{\tau}} = \frac{v_C(T)}{R_E}\frac{e^{-\frac{\Delta t}{\tau}}}{1-e^{-\frac{T}{\tau}}} \quad (20)$$

By plugging Equation 13 into equation 18 the simplified form is obtained:

$$\Delta i_S(T, \Delta t\ ) = \frac{V_0}{R_D+R_E} \cdot \frac{R_D}{R_E} \cdot e^{-\frac{T}{\tau}}\left[\frac{1-e^{\frac{-\Delta t}{\tau}}}{1-e^{-\frac{T}{\tau}}}\right] \quad (21)$$

Equation 21 reveals that the STP response is strongly damped in one of the following cases when:

a) $R_E >> R_D$;

b) $T >> \tau$;

c) the duty cycle is very small, $\Delta t/T \to 0$.

These observations lead us to conclude that:

- The induction of STP requires either high ionic strength electrolyte solution to make R_E small, or an active material with high resistance R_D, for instance an organic semiconductor instead of the usual organic conductor;
- Capacitance C_D must be large, thus large area electrodes with small channel, else high surface area nanostructured electrodes, may perform better (albeit as C_D increases also R_D decreases).
- For each τ there is a threshold pulse frequency;
- Judicious doping to increase R_D can be used for tailoring STP.
- The STP response is larger at small *T/t*, but a greater number of voltage pulses is needed to observe it.

- There is an optimum period T_s that maximizes $\Delta i_S(T_s, \Delta t)$.

These aspects will be systematically studied in a forthcoming publication.

4. Conclusions

We demonstrated that the current response of a device made of two PEDOT:PSS electrodes is selective for DA even without specific recognition moieties. The dynamic measurement of the STP transient current allows us to discriminate DA from other chemical species that are produced from DA metabolic and catabolic pathways. The breakthrough is in recognizing that the STP decay time τ_{STP} is a characteristic parameter of a given solute, which allows us to parametrize it in terms of a power law of the concentration. If on one hand we expected differences in response between DA and anionic molecules because of the negative charges at a physiological pH, we were positively surprised about the fact that DA gives rise to time scales substantially different than those of other cationic species, as from what we demonstrated in our previous works; in fact, HVA and DOPAC signals are 4 times lower with respect to the cationic DA. The important result here was to demonstrate that there is also a substantially different response also for the cationic catabolites and neurotransmitters, that exhibit just small structural differences with respect to DA like one methyl or hydroxyl group. The DFT calculations on a simple model of PEDOT:PSS binding DA or the cationic metabolites individually confirmed that DA gives rise to the strongest non covalent interaction with PEDOT:PSS followed by 3-MT, NE and EPI, respectively. Then we demonstrated with a simple adaptation of Eyring theory to the desorption of the interacting molecules with PEDOT:PSS, that an exponential correlation exists between the signal and the binding energy, although is not an ideal Arrhenius due to the distribution of the binding energies in PEDOT:PSS. This correlation, with the caveat that neglects other important phenomena like diffusion across a multiscale porous material like PEDOT:PSS, hint a simple way to rationalize the observed

sequence of the timescales, as well as the microscopic origin of the selectivity, viz. an exponential response to binding energies that may differ of a few kcal/mol

In order to better understand the origin of these differences in STP, we have solved a simple RC circuit pulsed with train of square pulses, to show that the current response is very much alike the one produced by our artificial synapse, and that the timescale τ depends on the capacitance and the in-series resistances of the circuit. The simplest rationale of this approach as a new sensing framework then lies in the change of the resistance and capacitance of the PEDOT:PSS interface by the different interactions with the solute present in the electrolyte solution. A more physical description should keep into account the dynamics of ions in and out of the PEDOT:PSS film, thus introducing time-varying capacitance and resistance. At the present level, we are assuming that their "mean" values account semi-quantitatively for the observed STP behavior. The value of this simple model is on the indication of sensitive parameters that would allow one to enhance the STP response. The important message from the simple circuit is that the STP response is not obtained always, but only at some "sufficiently high" frequency, and some rough figures of merit for the parameters are identified.

The novelty and relevance of this work lie in the demonstration that is possible to make selective sensor devices based on non-covalent interactions also in the absence of recognition groups coupled to the active elements of the device. This recognition scheme is completely general, since it requires first a different partition of the solute between the solution and PEDOT:PSS, and then different ion dynamics in and out the polymeric electrodes. The exponential correlation between the experimental STP timescale and the binding energy of DA metabolites interacting with PEDOT:PSS indicates that the slower dynamics of ionic species in and out PEDOT:PSS upon voltage pulsing might be the origin, or an important contribution, of the neuromorphic STP response of the device. Our sensing framework can discriminate differences of non-specific interactions with the active material as small as a few kcal/mol, else corresponding to

one functional group in the molecular structure. However, we cannot assess at this level other important effects related for instance to the dynamics/transport of the relevant molecule from/to the electrolyte to the PEDOT:PSS active binding sites.

Our observation and the rationale behind it suggest that homolog series of a certain species (e.g. alcohols, aldehydes or carboxylic acids with different chain lengths and/or steric hindrance), could be discriminated within their group due to this exponential amplification into the transient current of small differences in the binding energy with PEDOT:PSS. We may expect that by changing the counterion, it would be possible to extend this new type of spectroscopic sensing to other homolog families, also not endowed with H-bond forming moieties. Potential benchmark systems include perfluorinated compounds and aromatic molecules. It is also likely that an optimum frequency, that maximizes the differential STP response for each molecule of interest, exists and that the approach could be viable to identify "spectroscopically" the target analytes. In this respect, a seemingly relationship must exist between the response of STP sensors, driven at one frequency, and electrochemical impedance spectroscopy.

Supporting Information
Supporting Information is available from the Wiley Online Library or from the author.

Acknowledgements

This work was funded by the Life Science Department and by the Biomedical, Metabolic and Neural Sciences Department of University of Modena and Reggio Emilia, through "FAR 2015" and "FAR 2018", and by Regione Emilia-Romagna through "Percorso co-finanziato con risorse del Fondo Sociale Europeo Programma Operativo 2014/2020".

References

[1] W. Oertel, J. B. Schulz, *J. Neurochem.* **2016**, *139*, 325.

[2] J. Jankovic, *J. Neurol. Neurosurg. Psychiatry* **2008**, *79*, 368.

[3] P. Wester, U. Bergström, A. Eriksson, C. Gezelius, J. Hardy, B. Winblad, *J. Neurochem.* **1990**, *54*, 1148.

[4] E. S. Markianos, I. Nyström, H. Reichel, N. Matussek, *Psychopharmacology (Berl).* **1976**, *50*, 259.

[5] B. J. Venton, H. Zhang, P. A. Garris, P. E. M. Phillips, D. Sulzer, R. M. Wightman, *J. Neurochem.* **2003**, *87*, 1284.

[6] H. Fedorow, F. Tribl, G. Halliday, M. Gerlach, P. Riederer, K. L. Double, *Prog. Neurobiol.* **2005**, *75*, 109.

[7] H. Tang, P. Lin, H. L. W. Chan, F. Yan, *Biosens. Bioelectron.* **2011**, *26*, 4559.

[8] D. L. Robinson, B. J. Venton, M. L. A. V Heien, R. M. Wightman, *Clin. Chem.* **2003**, *49*, 1763.

[9] J. A. Johnson, R. M. Wightman, *Electrochem. Soc. Interface* **2017**, *26*, 53.

[10] K. Tybrandt, S. B. Kollipara, M. Berggren, *Sensors Actuators, B Chem.* **2014**, *195*, 651.

[11] I. Gualandi, D. Tonelli, F. Mariani, E. Scavetta, M. Marzocchi, B. Fraboni, *Sci. Rep.* **2016**, *6*, 35419.

[12] S. Casalini, F. Leonardi, T. Cramer, F. Biscarini, *Org. Electron.* **2013**, *14*, 156.

[13] F. Alibart, S. Pleutin, O. Bichler, C. Gamrat, T. Serrano-Gotarredona, B. Linares-Barranco, D. Vuillaume, *Adv. Funct. Mater.* **2012**, *22*, 609.

[14] Y. van de Burgt, A. Melianas, S. T. Keene, G. Malliaras, A. Salleo, *Nat. Electron.* **2018**, *1*, 386.

[15] Y. Kim, A. Chortos, W. Xu, Y. Liu, J. Y. Oh, D. Son, J. Kang, A. M. Foudeh, C. Zhu, Y. Lee, S. Niu, J. Liu, R. Pfattner, Z. Bao, T.-W. Lee, *Science (80-.).* **2018**, *360*, 998.

[16] M. Giordani, M. Di Lauro, M. Berto, C. A. Bortolotti, D. Vuillaume, H. L. Gomes, M.

[17] M. Giordani, M. Berto, M. Di Lauro, C. A. Bortolotti, M. Zoli, F. Biscarini, *ACS Sensors* **2017**, *2*, 1756.

[18] I. Gualandi, M. Marzocchi, E. Scavetta, M. Calienni, a. Bonfiglio, B. Fraboni, *J. Mater. Chem. B* **2015**, *3*, 6753.

[19] J. Granot, *FEBS Lett.* **1976**, *67*, 271.

[20] D. S. Goldstein, C. Holmes, Y. Sharabi, *Brain* **2012**, *135*, 1900.

[21] A. M. Nardes, M. Kemerink, R. A. J. Janssen, J. A. M. Bastiaansen, N. M. M. Kiggen, B. M. W. Langeveld, A. J. J. M. Van Breemen, M. M. De Kok, *Adv. Mater.* **2007**, *19*, 1196.

[22] D. C. Jimerson, M. D. Lesem, W. H. Kaye, T. D. Brewerton, *Arch. Gen. Psychiatry* **1992**, *49*, 132.

[23] N. J. Christensen, P. Vestergaard, T. Sørensen, O. J. Rafaelsen, *Acta Psychiatr. Scand.* **1980**, *61*, 178.

[24] J. M. L. Menon, C. Nolten, E. J. M. Achterberg, R. N. J. M. A. Joosten, M. Dematteis, M. G. P. Feenstra, W. H. (Pim) Drinkenburg, C. H. C. Leenaars, *J. Circadian Rhythms* **2019**, *17*, 1.

[25] E. Peskind, *Neuropsychopharmacology* **1998**, *19*, 465.

[26] A. Campana, T. Cramer, P. Greco, G. Foschi, M. Murgia, F. Biscarini, *Appl. Phys. Lett.* **2013**, *103*, 073302.

[27] M. Di Lauro, M. Berto, M. Giordani, S. Benaglia, G. Schweicher, D. Vuillaume, C. A. Bortolotti, Y. H. Geerts, F. Biscarini, *Adv. Electron. Mater.* **2017**, *3*, 1.

[28] F. Alibart, S. Pleutin, D. Guérin, C. Novembre, S. Lenfant, K. Lmimouni, C. Gamrat, D. Vuillaume, *Adv. Funct. Mater.* **2010**, *20*, 330.

[29] J. P. Perdew, K. Burke, M. Ernzerhof, **1996**, 3865.

[30] R. Ahlrichs, M. Bär, M. Häser, H. Horn, C. Kölmel, *Chem. Phys. Lett.* **1989**, *162*, 165.

[31] A. Klamt, *J. Phys. Chem.* **1995**, *99*, 2224.

[32] S. Grimme, J. Antony, S. Ehrlich, H. Krieg, *J. Chem. Phys.* **2010**, *132*, DOI 10.1063/1.3382344.

[33] R. Gangopadhyay, B. Das, M. R. Molla, *RSC Adv.* **2014**, *4*, 43912.

[34] A. Marutaphan, Y. Seekaew, C. Wongchoosuk, *Nanoscale Res. Lett.* **2017**, *12*, DOI 10.1186/s11671-017-1878-2.

[35] F. N. Ishikawa, M. Curreli, H. Chang, P. Chen, R. Zhang, R. J. Cote, M. E. Thompson, C. Zhou, *ACS Nano* **2009**, *3*, 3969.

[36] O. Bichler, W. Zhao, F. Alibart, S. Pleutin, D. Vuillaume, C. Gamrat, *IEEE Trans. Electron Devices* **2010**, *57*, 3115.

[37] S. Desbief, A. Kyndiah, D. Guérin, D. Gentili, M. Murgia, S. Lenfant, F. Alibart, T. Cramer, F. Biscarini, D. Vuillaume, *Org. Electron. physics, Mater. Appl.* **2015**, *21*, 47.

[38] J. Rivnay, P. Leleux, M. Ferro, M. Sessolo, A. Williamson, D. a. Koutsouras, D. Khodagholy, M. Ramuz, X. Strakosas, R. M. Owens, C. Benar, J.-M. Badier, C. Bernard, G. G. Malliaras, *Sci. Adv.* **2015**, *1*, e1400251.

[39] R. Kubo, *J. Phys. Soc. Japan* **1962**, *17*, 1100.

[40] N. G. Van Kampen, *Stochastic Processes in Physics and Chemistry*, North Holland, **2007**.